

ZnO/PSi nanoparticles thin film for NO₂ sensing application prepared by pulsed laser deposition

H A Radwan¹, J M Marei¹, A A Khalefa¹ and J M Rzaïj^{2*} 

¹Ministry of Education, Kirkuk, Iraq

²Department of Physics, College of Science, University Of Anbar, Ramadi, Iraq

Received: 03 January 2023 / Accepted: 02 June 2023 / Published online: 20 June 2023

Abstract: Zinc oxide nanoparticles (ZnO NPs) were deposited on porous silicon using pulsed laser deposition for nitrogen dioxide detection. A silicon wafer was electrochemically etched to produce a high-porosity surface for depositing ZnO nanoparticles. X-ray diffraction analysis revealed a single crystalline pattern for the Si substrate at a diffraction angle of 28.5° and a polycrystalline structure with a hexagonal phase of zinc oxide when the porous silicon was coated with the ZnO NPs. Field emission scanning electron microscopy demonstrated the transformation of single-crystal silicon into a porous structure. It revealed a high porosity surface with uniformly distributed pores of 1 μm diameter, while zinc oxide nanoparticles aggregated on porous silicon to form spherical nanostructures with particle sizes ranging from 23 to 54 nm. Photoluminescence analysis of electrochemically etched silicon showed a strong, broad, single-peak emission at 671 nm, while the zinc oxide-coated porous silicon exhibits emission peaks at 375, 542, 670, and 780 nm. NO₂ sensing investigations confirmed the enhanced sensitivity response of ZnO deposited on porous silicon compared to ZnO deposited on the silicon substrate. The developed NO₂ sensor displayed maximum selectivity and sensitivity (75.3%) at 100 °C operating temperature, with response and recovery time of 25 and 35 s, respectively, enhancing by about 2.6 times for the ZnO/PSi compared with the ZnO/Si sensor. The simplicity, low cost, and efficiency of the prepared sensors make them a good candidate for gas sensing applications.

Keywords: Zinc oxide; Nanoparticle; Gas sensor; Porous silicon; Pulsed laser deposition

1. Introduction

Chemiresistive gas sensors, particularly those based on metal oxides, have attracted many researchers for their ease of installation, low cost, and possible integration with control electronics [1]. These sensors depend on the principle of changing the electrical resistance of the sensor when exposed to the target gas due to the difference in the number of oxygen species adsorbed on its surface. The adsorbed oxygen ions capture the surface electrons from the conduction band. The change in sensor resistance occurs due to the interaction of the target gas with oxygen species adsorbed on the surface, causing variations in charge carrier concentration and mobility [2]. The sensitivity of the manufactured device varies according to the type of substance, the technology used in the deposition of

films, doping, or control of the nanostructure of the active substance [3]. Modifying the nanoparticle structure is one of the most important ways to enhance the efficiency of the sensor [4].

Porous silicon (PSi) has recently been proposed for gas sensors due to its unique properties. Using a simple and inexpensive method, the porosity of silicon samples, and thus the effective surface area exposed to the gas, can be significantly increased [5]. The PSi substrate is a crucial element in gas sensing applications owing to its notable characteristics such as high surface area, stability, and low operating temperature, which contribute to distinct sensing properties [6]. PSi has been widely used for various applications such as room temperature gas sensing, which has good dynamic properties, sensitivity, and high selectivity [7]. The porous silicon's physical structure is an impact factor in fabricating the porous surface using the electrochemical etching. The acid concentration used in the etching, the etching time, the current density, the porous

*Corresponding author, E-mail: sc.jam72al@uoanbar.edu.iq

area, and the length of the anodizing can all be employed to control the structure, thickness, and size distribution of the silicon pores. On the other hand, oxidation, nitridation, or even additional chemical treatments can modify the chemical properties of porous silicon surfaces for various applications [8].

Several semiconductor materials have been extensively investigated as sensor materials [9]. Zinc oxide is a type of semiconductor with a wide and direct energy gap of about 3.37 eV [10]. ZnO is included in many fields, such as gas sensors and photovoltaic applications [11]. Traditional ZnO-based gas sensors maintain challenges, including high operating temperatures, extended response-recovery time, and low selectivity. The limited activity of conventional ZnO sites prevents the adherence of oxygen atoms to the ZnO surface, reducing ZnO sensing features. So, the major goal of the research is to enhance the active sites of the ZnO sensor by modifying the sensing surface, shape, size, and nanostructure to improve the performance of ZnO sensors [12].

According to investigations by Zhang et al. [13], the thin layer's deposition method is a critical factor in determining the film device's performance, with each method or set of deposition parameters (such as surface porosity, average surface roughness, crystallite size, and film thickness) result in thin films with various micro- and macrostructures. ZnO thin films have been deposited using a variety of techniques, including chemical bath deposition [14], atomic layer deposition [15], and magnetron sputtering [16]. While these methods offer high-quality thin films, they often require toxic precursors and expensive equipment. Several low-cost techniques, including spray pyrolysis, spin coating [17], and sol-gel [18], have been employed for the deposition of thin films. However, these methods cannot precisely control the reproducibility and uniformity of film thickness. The PLD technique exhibits high efficiency compared to alternative methods due to its capability to produce high-quality films at reduced substrate temperatures. The PLD technique presents additional, such as performing deposition under influenced reactive gas pressure and achieving high deposition rates. The combined utilization of these factors facilitates accurate control of film composition and properties [19]. We utilized Pulsed Laser Deposition for depositing ZnO films on silicon substrates for this purpose. Numerous studies [20–23] have investigated undoped and zinc oxide doped with various materials for gas-sensing applications to detect various concentrations of toxic gases. Moreover, many studies [24–27] were achieved based on porous silicon for gas sensing applications. The earlier reports employed preparation methodologies associated with high costs and requiring meticulous monitoring. Furthermore, these reports did not consider the detection of nitrogen

dioxide or the fundamental interaction mechanism between the gas and the sensor's surface.

Nitrogen oxides, in monoxide (NO) and dioxide (NO₂) forms, are considered the most toxic gases due to their substantial impact on the environment and human health. Nitrogen oxides are recognized as atmospheric contaminants that give rise to acid rain and smog. Their existence poses a perilous threat to the sustenance of life, even when present in low concentrations [28]. The impetus behind our efforts to enhance the detection of this lethal gas is the driving force for this study. The investigation of the gas-surface interaction mechanism is essential to demonstrate the fluctuations in electrical conductivity of the active material of the sensor, which supports the development of a high-sensitive sensor [29]. In this work, PSi substrates were fabricated using electrochemical etching for ultra-thin ZnO layer deposition to enhance the NO₂ sensing characteristics. The morphological features of the produced sensor were examined to achieve rewards for PSi samples and to maintain porosity after ZnO deposition. Furthermore, the gas sensing characteristics of the developed sensor toward various NO₂ concentrations were investigated, and the sensing mechanism was discussed.

2. Experimental details

An electrochemical etching process was used to form a porous silicon layer onto (111) n-type silicon wafer using a Teflon cell sealed by rubber O-rings. The silicon wafer samples were cut into 15 × 15 mm² dimensions and ultrasonically cleaned in methanol before use. As shown in Fig. 1, the silicon wafer is connected as the anode, while the cathode electrode is made from platinum. A diluted hydro-fluoride solution (HF): distilled water of 1:2 ratio was used. A constant current of 15 mA was used at 10 min of etching time. Finally, the porous silicon is washed with deionized water and stored in containers in methanol. The ZnO target (Aldrich 99.9% purity) with a thickness of 0.7 cm and a diameter of 3 cm was installed 6 cm from the porous silicon substrate. The ZnO target was evaporated under a 10⁻² kPa vacuum using a pulsed ND-YAG laser with a wavelength of 1064 nm, a pulse frequency of 2 Hz, a pulse duration of 10 ns, a focal spot width of 2 mm, and a pulse energy of 400 mJ. The target was installed on a rotating holder to prevent rapid drilling, as seen in Fig. 2. A mesh of aluminium electrodes was deposited on the samples by thermal evaporation under a high vacuum using the Edward Coating system. The performance of the developed gas sensors was evaluated in a closed vacuum chamber. The chamber base has a temperature-controlled heater to determine the sensor's operating temperature. The gas target and air mixture flow into the chamber by two

Fig. 1 The schematic representation of the system utilized for forming the porous silicon layer

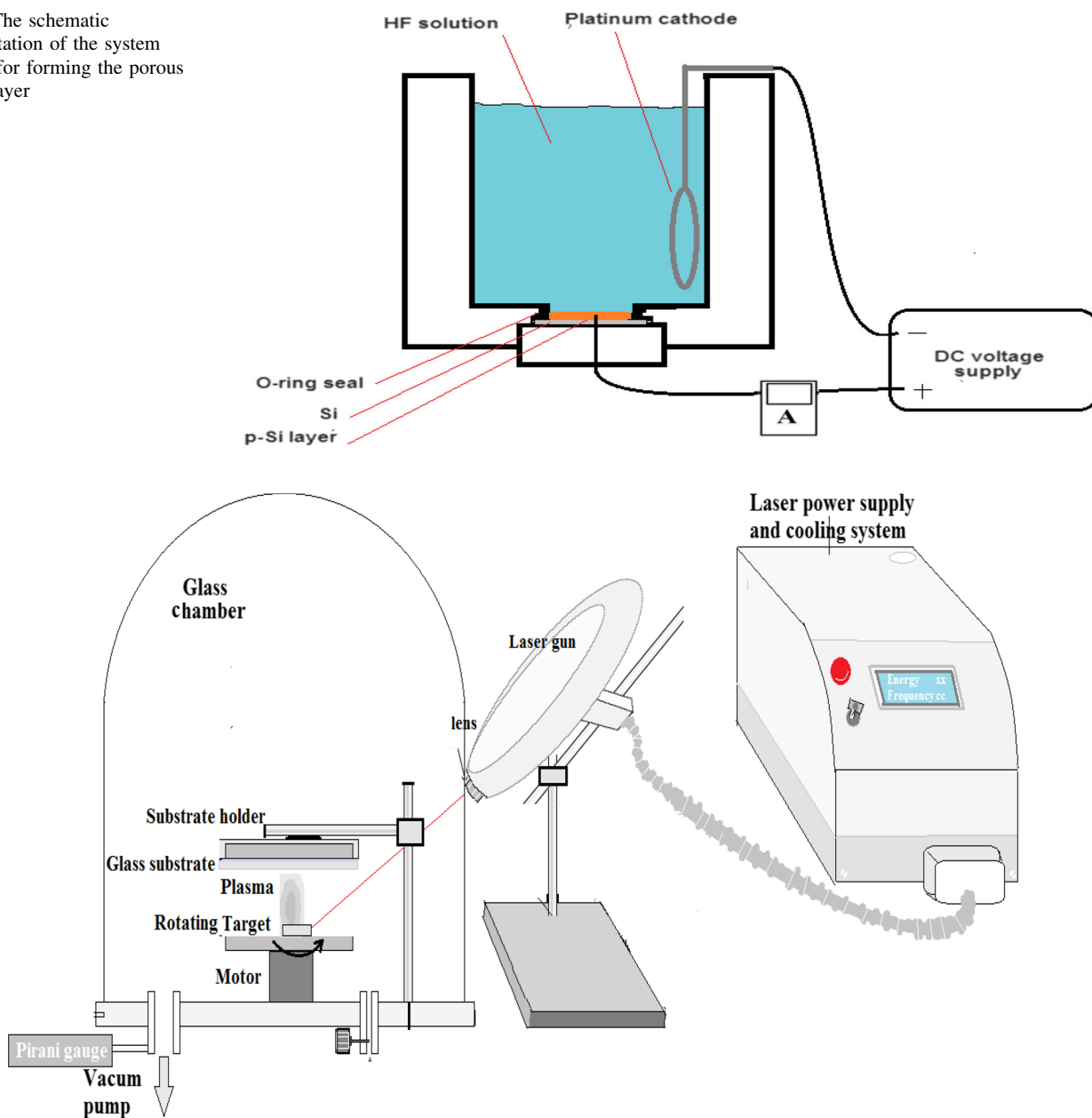


Fig. 2 The schematic representation of the employed pulsed laser deposition technique

flow-meter. When the sensor was alternately exposed to a specific concentration of the gas target and then air, the sample resistance was measured as a function of time using a multimeter connected to a computer. The thickness of the prepared samples was determined via gravimetric analysis. The results indicate that the thickness of the zinc oxide sample deposited on the silicon (ZnO/Si) was approximately 123 nm, while the sample deposited on the porous silicon (ZnO/PSi) was 103 nm.

3. Characterization of nanostructured ZnO

The structural properties of the films were analyzed using an X-ray diffractometer (6000 Shimadzu, Cu-K α target, wavelength of 54,060 Å, Voltage of 40 kV, speed of 5°/min, and Current of 30 mA). The surface microstructure and pore size distribution were analyzed using a field emission scanning electron microscope, a type of FEI-Netherlands with a 300,000X magnification. EDS (Energy-Dispersive X-ray Spectrometer) was used for surface elemental analysis. A dynamic gas flow system of a chemoresistive sensor setup was employed to analyze the

sensitivity of the developed samples against various concentrations of nitrogen dioxide. The target gas's ambient atmosphere was a mix of synthetic air and nitrogen dioxide provided by Air Products, Iraq.

4. Results and discussions

The X-ray diffraction patterns for the silicon wafer and the porous silicon layer are displayed in Fig. 3. A single crystalline Si pattern appeared for the Si with a single peak at about $2\theta = 28.5^\circ$ for (111) Si direction, according to the standard card No. 96–901-3108. After etching, this peak appeared as a broad feature with lower intensity than the started sample at nearly the exact diffraction angle. Figure 4 illustrates the XRD pattern for the nanocrystalline ZnO deposited on the porous silicon (P-Si) compared with the standard lines for the ZnO hexagonal structure (card No. 96-901-1663). Figure 4 shows a polycrystalline structure with a hexagonal phase of a zinc oxide film with diffraction peaks (100), (002), (101), (102), (110), and (103) corresponding to the diffraction angles 28.500° , 31.809° , 34.452° , 36.293° , 47.575° , 56.644° , and 62.893° respectively, in addition to the broad peak at $2\theta = 28.5^\circ$ for the (111) P-Si diffraction peak with a cubic system. This broad feature of the diffraction pattern indicates the successful deposition of nanocrystalline ZnO particles on the P-Si layer. The prepared sample's crystallite size (D) was calculated using the Debye–Scherrer formula (Eq. 1) [30], and it was found that the average crystal size was 22 nm. The lattice constants of the ZnO/PSi film were calculated and found to be $a = b = 3.2472 \text{ \AA}$ and $c = 5.2045 \text{ \AA}$. The

peaks broadening for ZnO were determined by Lorentzian fitting and corrected by subtracting $K\alpha_2$, and instrument broadening effects using X-powder software, as shown in Fig. 5.

$$D = \frac{k\lambda}{\beta\cos\theta}, \quad (1)$$

where λ , β , and θ are the wavelength of the $\text{CuK}\alpha$ line, FWHM of the diffraction peak, and the Bragg diffraction angle, respectively.

Table 1 reveals the diffraction angles (2θ), Full width at half maximum (FWHM), interplanar spacing (d_{hkl}) calculated using Bragg's law, the crystallite size (D) calculated by Sherrer's formula, and corresponding Miller indices for the ZnO film that was deposited on porous silicon.

The pores morphology is easily adjustable during fabrication, allowing for pore width and length design. The pore shape has a direct impact on the specific area. Regarding sensing devices, the specific area is the accessible area exposed to the target gas. The physisorption of the target gas molecules interacts with the specific area, affecting the optical or electrical properties of the porous silicon. So, a larger specific area would result in a more sensor response, and the strength of the sensor response is dependent not only on the specific area but also on the type of silicon conductivity [27].

The etched silicon layer was analyzed using Field Emission Scanning Electron Microscopy (FE-SEM). Figure 6 displays the FE-SEM images of the layer, including a top view at two different magnifications (a and b) and a cross-section view at two different magnifications (c and d). The top-view micrograph images revealed a high

Fig. 3 X-ray diffraction patterns and peak profile fits of Si substrates (a) before and (b) after electrochemical etching

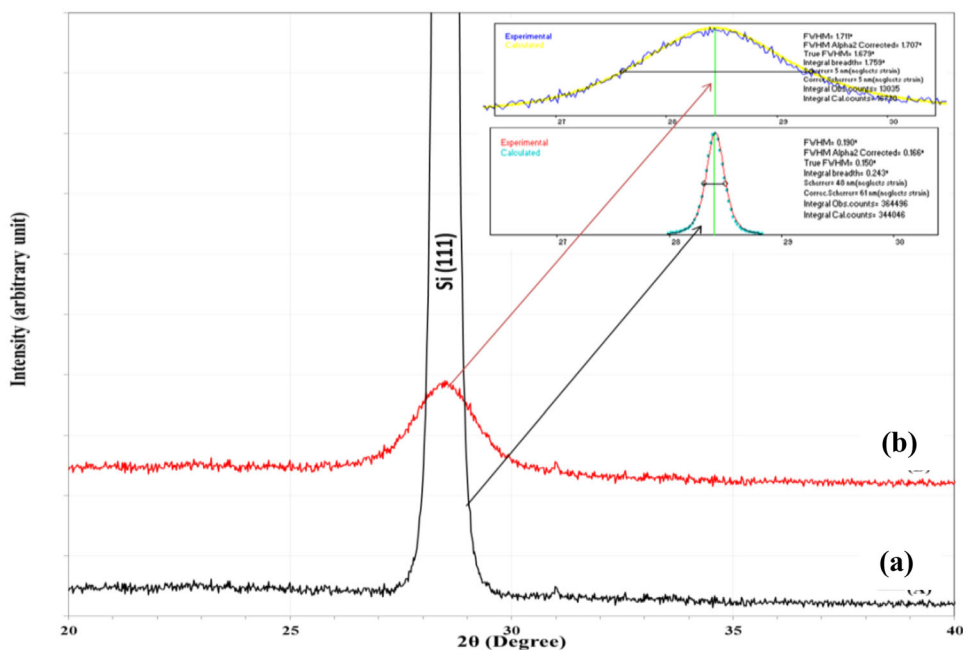


Fig. 4 X-ray diffraction pattern of ZnO/PSi thin film

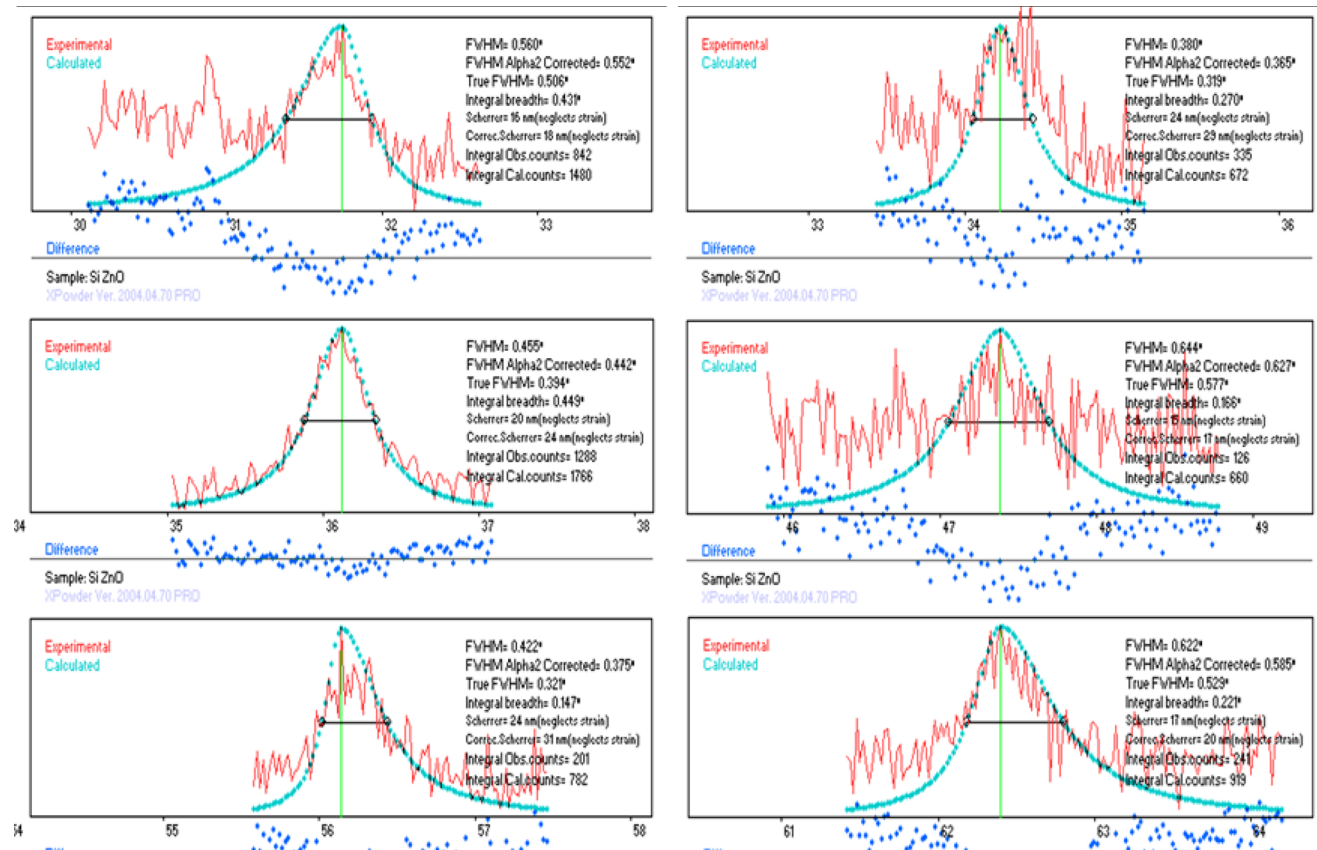
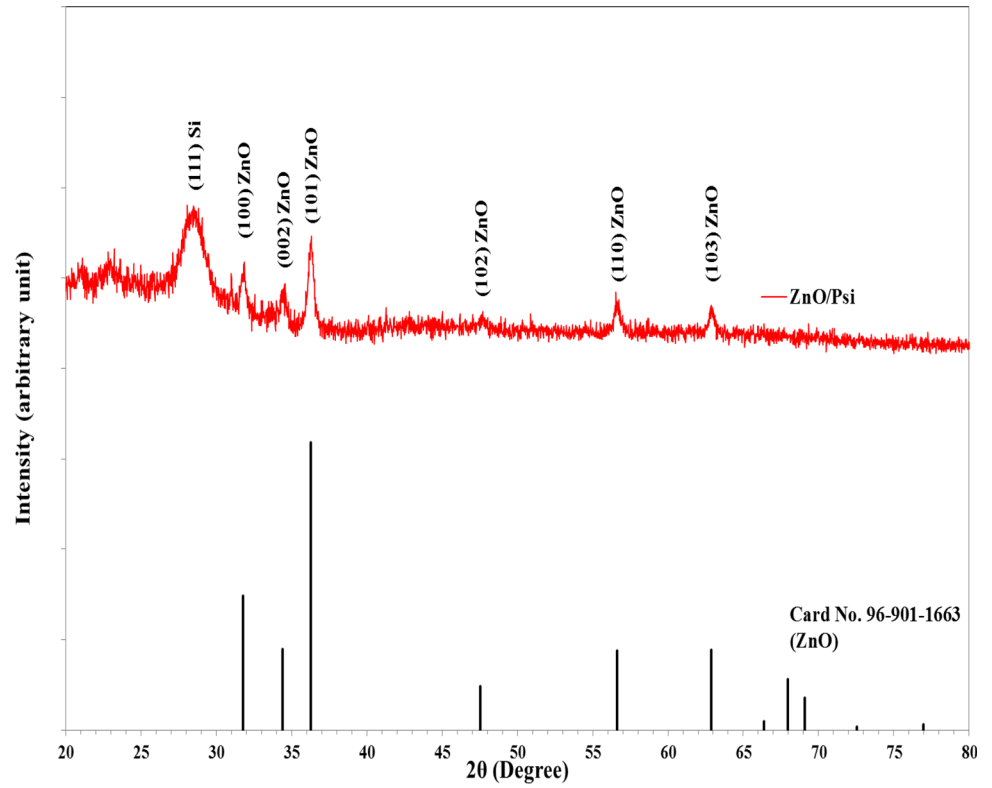


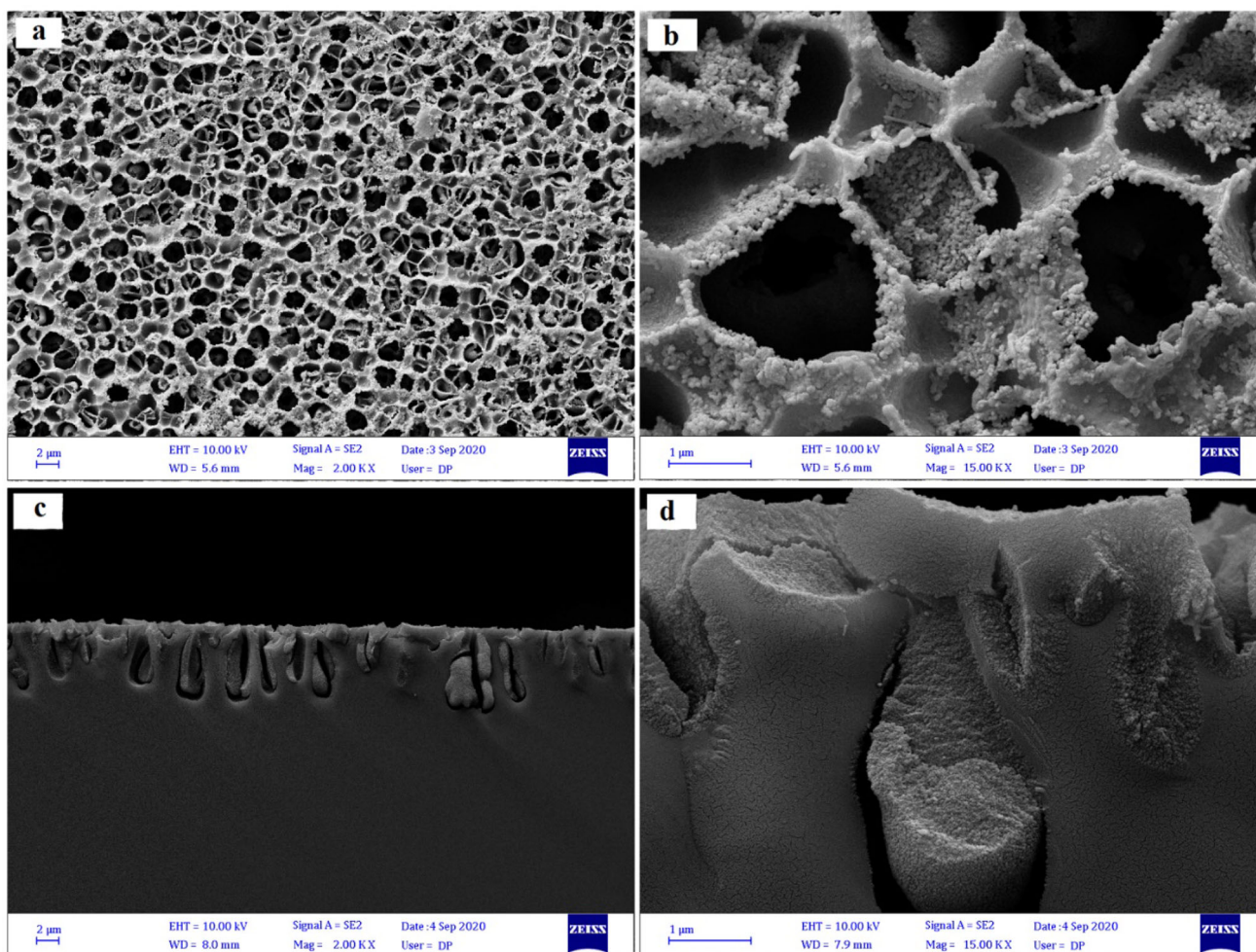
Fig. 5 Lorentzian fitting of the ZnO diffraction peaks

Table 1 XRD parameters of ZnO/PSi thin film

2 θ (Deg.)	FWHM (Deg.)	d_{hkl} (Å)	D (nm)	hkl	Phase
28.500	1.670	3.129	4.9	(111)	Cub. Si
31.809	0.506	2.811	16.3	(100)	Hex. ZnO
34.452	0.319	2.601	26.1	(002)	Hex. ZnO
36.293	0.394	2.473	21.2	(101)	Hex. ZnO
47.575	0.577	1.910	15.1	(102)	Hex. ZnO
56.644	0.321	1.624	28.1	(110)	Hex. ZnO
62.893	0.221	1.477	42.1	(103)	Hex. ZnO

porosity surface with uniformly distributed pores. The pore diameter was estimated using ImageJ software, and it was found in the range of 1 μm . Figure 7(a) depicts the FE-SEM image of ZnO nanoparticles deposited on Si substrate, magnified at 50000x, while Fig. 7(b) presents the histogram of the nanoparticle size distribution. The histogram depicts a uniform particle size distribution, ranging

from 39 to 89 nm, with an average of 53 nm. The micrograph images presented in Fig. 8 depict the surface of porous silicon coated with zinc oxide nanoparticles, at magnifications of 2000x (Fig. 8a) and 30000x (Fig. 8b). It demonstrates that the zinc oxide nanoparticles were aggregated into spherical nanostructures with sizes between 23 and 54 nm. Figure 8(a) also reveals polygonal pores with diameters ranging between 0.5 and 1 μm separated by thin walls with a thickness of up to 100 nm. This structure of a large surface area is adequate for gas-sensing applications. The porous surface with a large area is reported to be effective in applying the gas sensor because it increases the surface area exposed to the target gas and subsequently increases the sensor's response [31]. Figure 9 shows the EDX map for the ZnO thin layer on porous silicon. The EDX map shows the uniformly distributed Si and Zn over the surface of the sample. The oxygen element (O) appeared distributed over the entire surface with high density compared with the other elements due to the

**Fig. 6** FE-SEM images of the etched silicon layer at two magnifications: (a) and (b) top view, (c) and (d) cross-section view

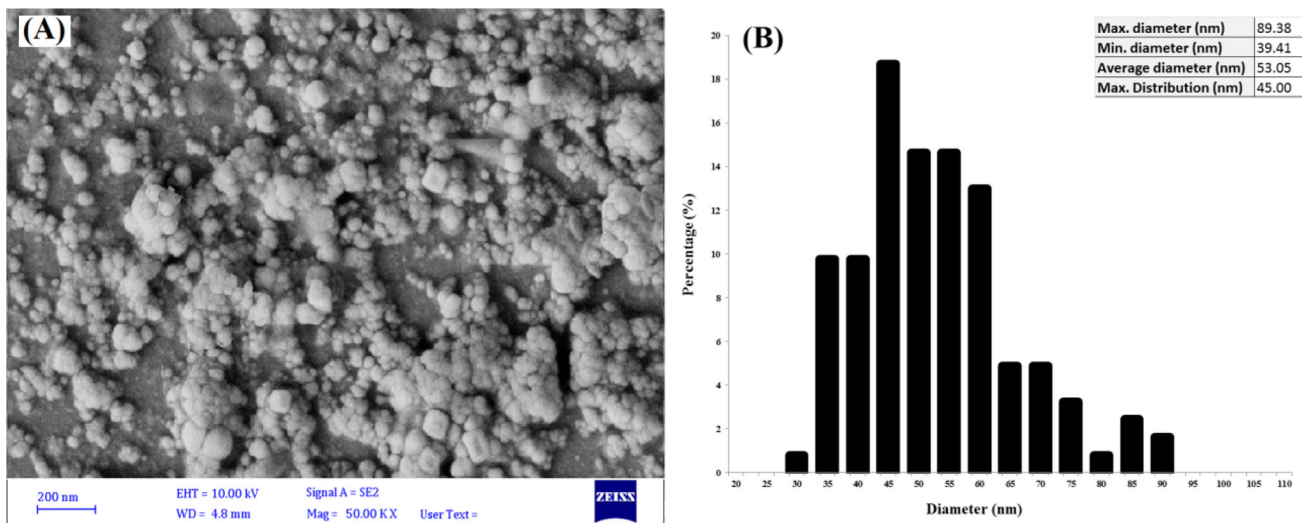


Fig. 7 FE-SEM images of ZnO nanoparticles (a) top view and (b) size distribution

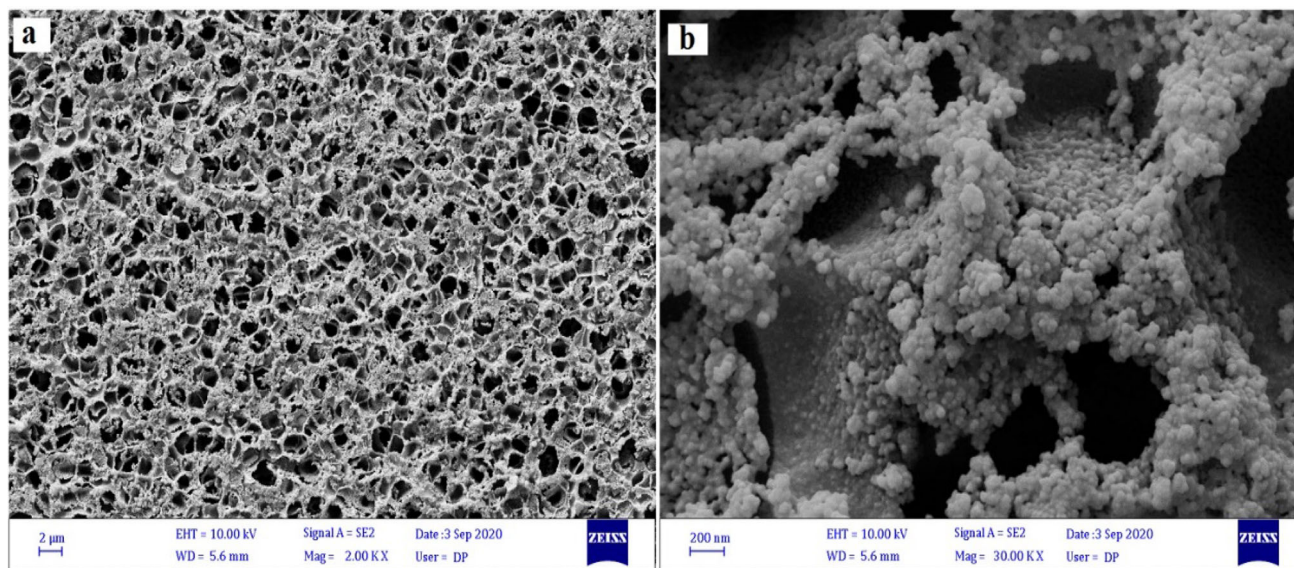


Fig. 8 Top-view FE-SEM micrographs of ZnO/PSi at magnifications of (a) 2kx and (b) 30kx

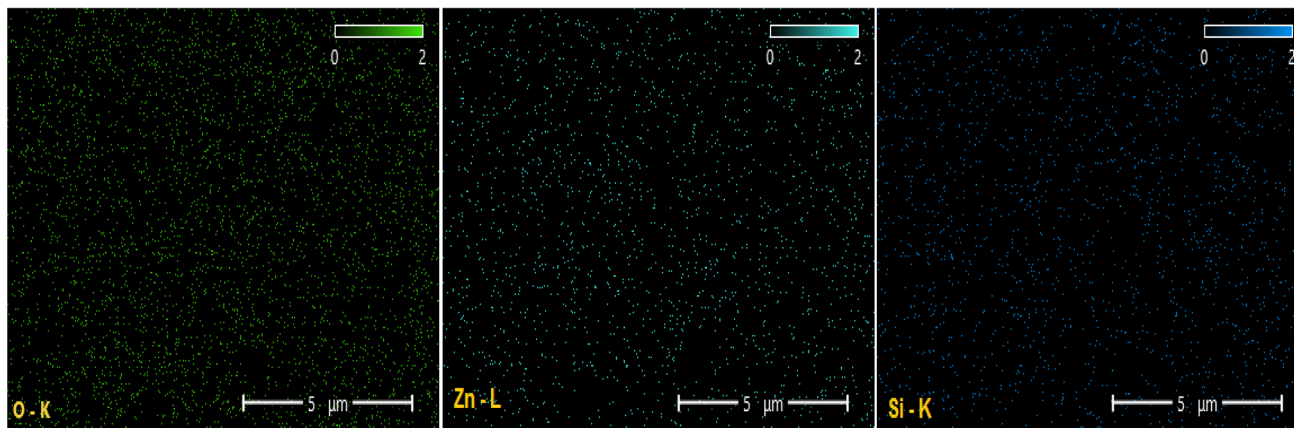


Fig. 9 EDX map of ZnO-coated-porous silicon

porosity procedure effect and also comes from oxygen in the deposited ZnO.

The study of the photoluminescence (PL) spectrum of nano/microstructures of porous silicon and the effect of ZnO nanoparticles on the features of this spectrum is essential in determining the properties of gas sensing devices since it has a direct effect on the properties of deposited films [32]. A PL fingerprint in a semiconductor is often composed of near-band-edge emission and defects-related luminescence. Near-band-edge emission is attributed to the recombination of free-charge carriers (electrons-holes) with bound charge carriers (holes-electrons), which are referred to as free-to-bound (FB) transitions. The photoluminescence emission spectrum associated with defects is caused by (a) recombination between donor electrons of the semiconductor and acceptor holes, (b) recombination between conduction band electrons of the semiconductor and acceptor holes, and (c) recombination of donor electrons to the valence band of the semiconductor.

Figure 10 depicts the photoluminescence spectrum of uncoated and porous silicon coated with zinc oxide nanoparticles. The photoluminescence (PL) spectrum of the porous silicon developed in this study is presented in Fig. 10(a). The spectrum exhibits a broad red luminescence band centered at a wavelength of 671 nm. This central wavelength corresponds to 1.84 eV ($E_g = 1240/\lambda$), related to the energy gap of the etched silicon. Pavlenko et al. [33] investigated the biphotonic applications of ZnO on porous silicon. They reported that the energy gap of the etched silicon was 1.85 eV, which corresponds well with our

findings. This band, known as the S-band, is caused by carriers' 2-D quantum confinement, increasing the Si bandgap. This band can be adjusted depending on the PSi preparation conditions and related to changes in nanostructures or the creation of new electronic states from the Si-O bond due to varying oxidation levels. Radiative decay lifetime data suggested that the high PL efficiency of PSi was due to the low probability of identifying a nonradiative recombination center in Si nanocrystallites [34]. Figure 10(b) indicates an enhancement in the PL spectrum of the ZnO/PSi by widening the luminescence spectrum due to the ZnO nanoparticle deposition [35]. The ZnO/PSi exhibits an emission peak centered at 375 nm and three peaks at 542, 670, and 780 nm. The observed PL peak in the ultraviolet region at a wavelength of 375 nm is ascribed to the excitonic emission arising from the transition between the near conduction and valence bands. This finding supports the determination of the energy gap of ZnO to be 3.3 eV, consistent with the finding obtained by Wei et al. [36]. In contrast, the blue-green emission band peak (542 nm, 2.28 eV) has been reported as the most common band for ZnO, typically attributed to the non-stoichiometric composition of ZnO (defects mainly due to oxygen vacancies) [37]. The band at the IR range (780 nm, 1.6 eV) referred to dangling bonds in porous silicon defect-related emission [38].

Electrical resistance variations versus time at various operating temperatures (27 (RT), 100, 150, and 200) °C for ZnO on Si (ZnO/Si) and ZnO on porous Si (ZnO/PSi), respectively, are shown in Figs. 11 and 12 to illustrate the effect of the porous surface on the gas sensitivity results of

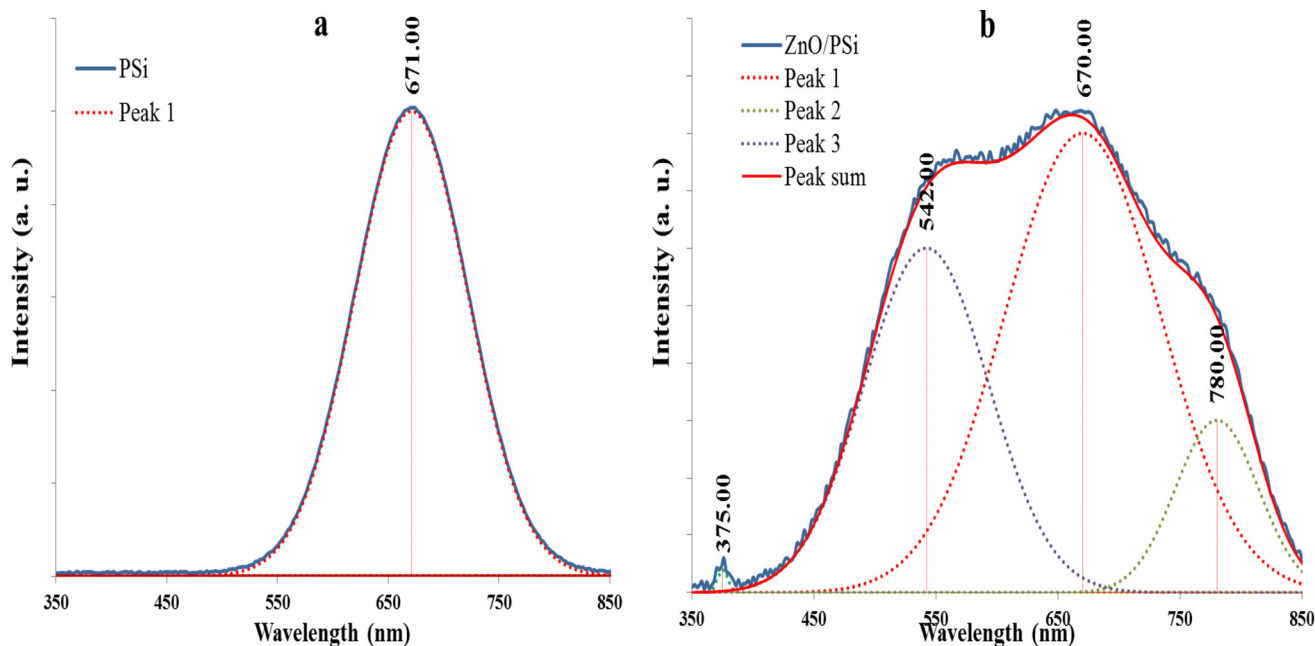


Fig. 10 PL spectrum of (a) electrochemically etched silicon substrate and (b) ZnO/PSi

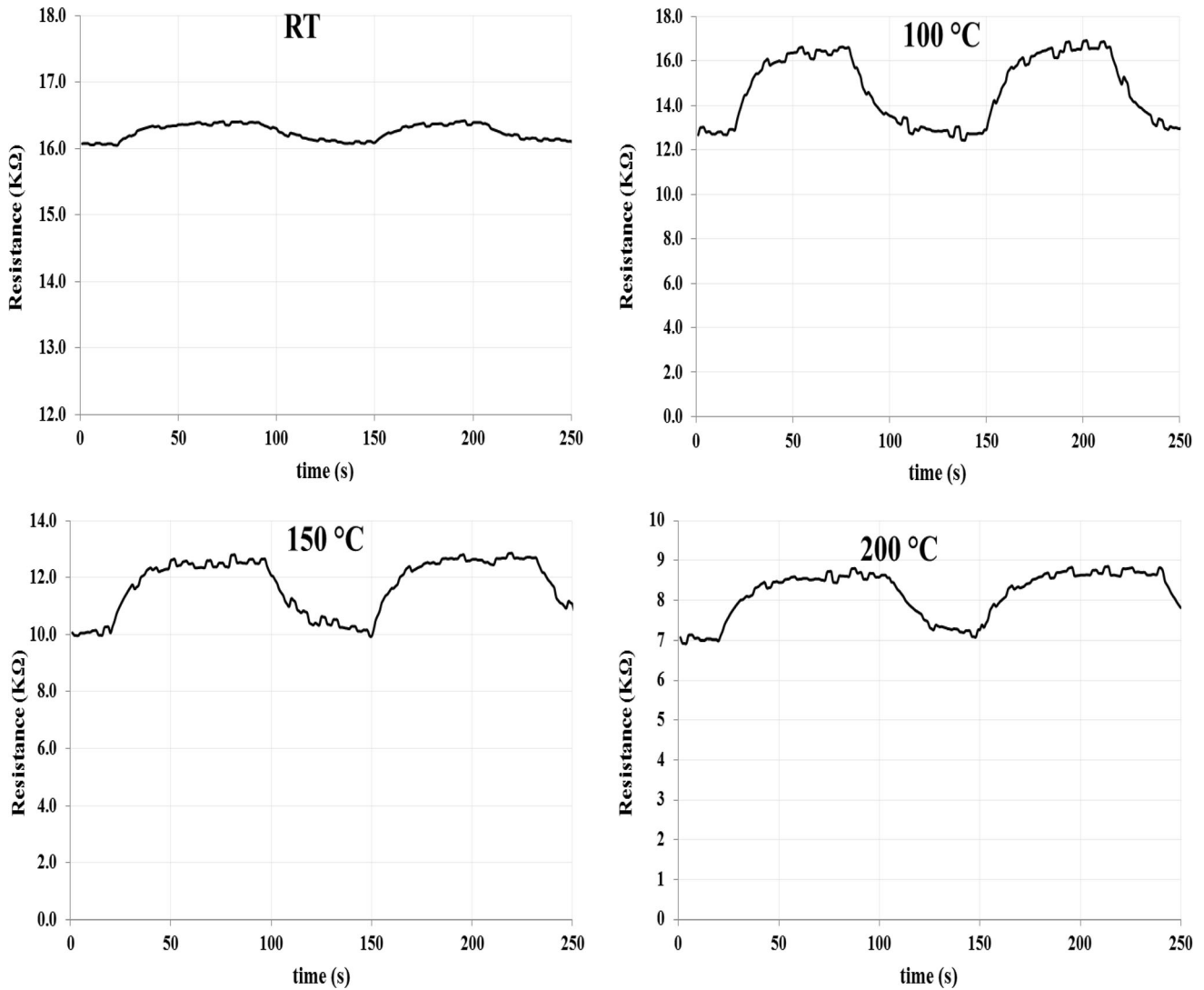


Fig. 11 Variation in ZnO/Si sensor resistance at various operating temperatures

the deposit zinc oxide film. Figures 11 and 12 indicate that when the ZnO film surface was exposed to 5 ppm NO₂, the electrical resistance increased, whereas resistance decreased when the target gas was removed. An ionic reaction between NO₂ gas molecules and oxygen on the surface causes the extraction of electrons from the n-type semiconductor (ZnO), decreasing the conductivity of the ZnO and increasing electrical resistance [3]. Figures 11 and 12 demonstrate that the response of the two prepared samples differed depending on the surface morphology of each sensor. Specifically, the ZnO/PSi-based sample exhibited a more significant response than the ZnO/Si sensor. The sensitivity (S%) of the sensor is calculated using Eq. 2.

$$S\% = \frac{|\Delta R|}{R_{\text{air}}}, \quad (2)$$

where $|\Delta R| = |R_{\text{gas}} - R_{\text{air}}|$ is the resistance variation, and R_{gas} and R_{air} are the sample resistance in the target gas and air respectively [39]. Figure 13 shows the sensitivity variation at an operating temperature varied from room temperature (25 °C) to 300 °C for ZnO/Si and ZnO/PSi sensors. The sensitivity of ZnO on PSi enhanced compared with the ZnO deposited on Si. The porous surface of the sensor layer increases gas target molecule exposure, enhancing the adsorption rate and sensing properties. The surface characteristics and nanostructure of thin films typically influence gas-sensing components by raising the ratio of surface area to volume [40].

To improve the sensor's response, determining the operating temperature is an influential factor since, at this temperature, the required activation energy on the sensor's surface is sufficient to complete the chemical reaction process [41]. The optimum sensitivity appeared at 100 °C

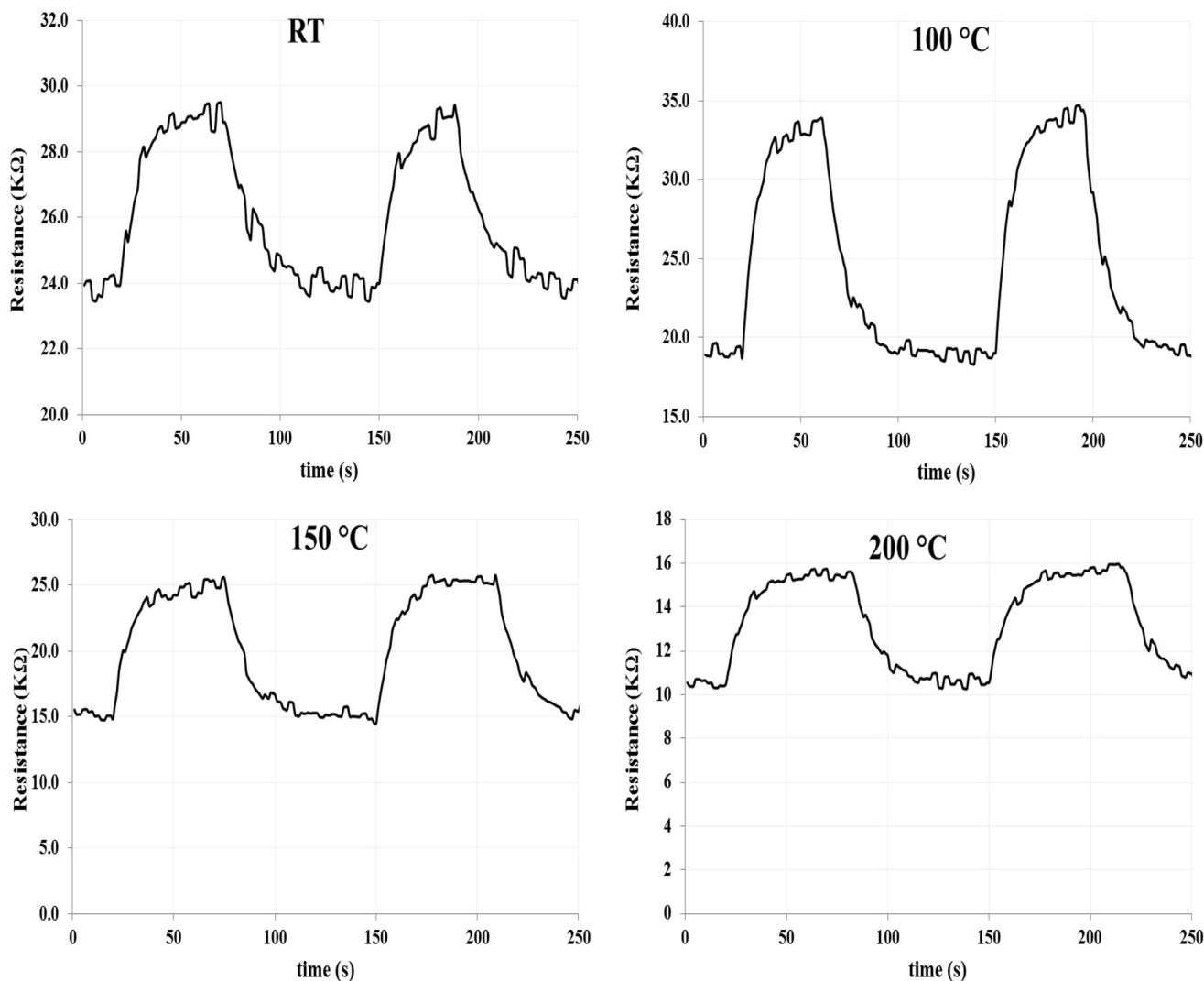
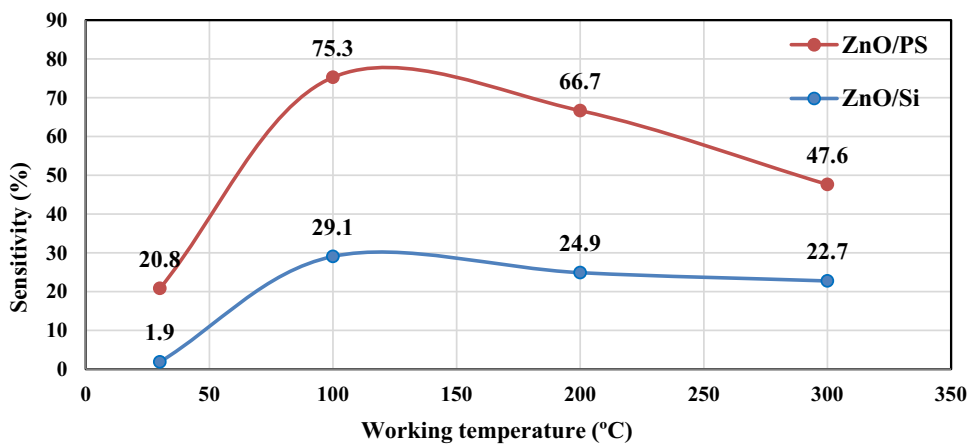


Fig. 12 Variation in ZnO/PSi sensor resistance at various operating temperatures

Fig. 13 ZnO/Si and ZnO/PSi sensor sensitivity to 5 ppm NO₂ as a function of working temperature

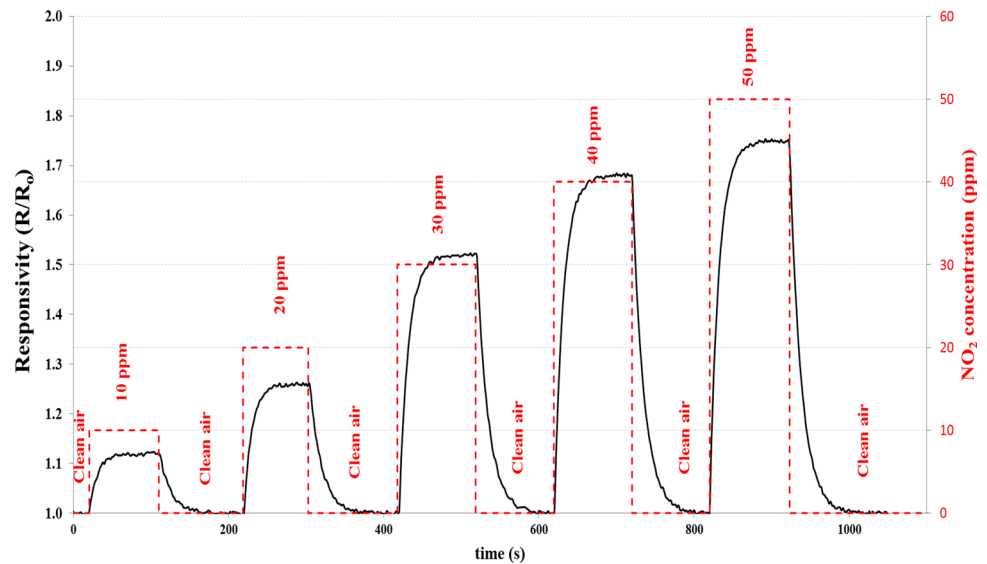


for the two prepared sensors. The sample response variation with the applied temperature due to the variation of dominant oxygen species contributes to the sensitivity

mechanism that is adsorbed on the sample surface. At low temperatures, O₂⁻_{ads} are the dominant ones adsorbed from the ambient and attract electrons from the surface atoms'

Table 2 Sensitivity, response time, and recovery time for ZnO/Si and ZnO/PSi sensors

Sensor	Temp. (°C)	Sensitivity%	Response time (s)	Recovery time (s)
ZnO/Si	27	1.9	37.0	58.0
	100	29.1	32.0	45.0
	200	24.9	39.0	52.0
	300	22.7	42.0	52.0
ZnO/PSi	27	20.8	29.0	45.0
	100	75.3	25.0	35.0
	200	66.7	30.0	40.0
	300	47.6	33.0	40.0

Fig. 14 ZnO/PSi sensor response against 10–50 ppm NO₂ at 100 °C

conduction band, creating a depletion region. Increasing temperature cause the dissociation reaction $O_{2ads}^- + e^- = 2O_{ads}^-$ [42], which attracts more electrons from the sample, and the O_{ads}^- be dominant. While increasing temperature cause to reduce the adsorbed gases on the sample surface and reduce the sample response [43]. The response and recovery time, important specification parameters for gas sensors, were determined and listed in Table 2. At a temperature of 100 °C, the ZnO/PSi and ZnO/Si exhibited response times of 25 and 32 s, respectively, displaying the lowest response time. The response time revealed a shorter response than recovery times for all samples due to slow desorption reactions compared to the rapid desorption process [44]. Table 2 illustrates gas sensitivity, response time, and recovery time for ZnO/Si and ZnO/PSi sensors against NO₂ gas at different operating temperatures.

In contrast to minimum response and recovery times, the two sensors' maximum sensitivity appeared at 100 °C. The sensitivity enhanced about 2.6 times for the ZnO/PSi compared with the ZnO/Si sensor. Figure 14 depicts the

dynamic response (R_{gas}/R_{air}) [45] of the ZnO/PSi sensor when subjected to varied NO₂ concentrations ranging from 10 to 50 ppm mixed with air at 100 °C. This figure indicates that the sensor response improved when the NO₂ concentration increased. When the gas concentration increases, the number of NO₂ molecules interacting with oxygen ions increases, causing an increase in the potential barrier at grain boundaries, preventing more charge carriers' transformation and increasing resistance [46]. Based on the sensor sensitivity results, a relationship between sensitivity and gas concentration can be hypothesized using Eq. 3. Figure 15 confirms that the R² value (0.9856) corresponds to the hypothesized gas concentration and sensitivity relationship.

$$y = -0.0179X^2 + 2.7414X - 15.8, \quad (3)$$

where y is the sensitivity and X is the gas concentration in ppm.

The sensitivity of the ZnO/PSi sensor in response to 10 ppm of nitrogen dioxide (NO₂), carbon dioxide (CO₂), and sulfur dioxide (SO₂) at varying operating temperatures

Fig. 15 The sensitivity of the ZnO/PSi sensor in response to 10–50 ppm NO₂ concentrations

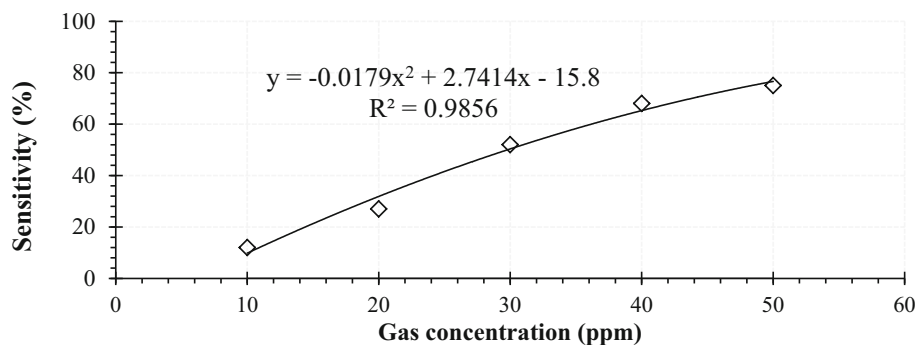
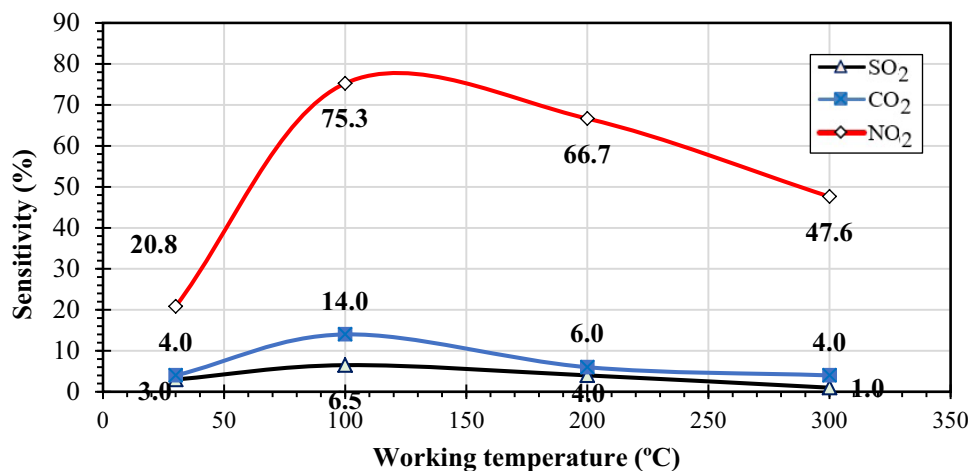


Fig.16 The sensitivity of the ZnO/PSi sensor to detect 10 ppm of NO₂, CO₂, and SO₂ at various operating temperatures



is shown in Fig. 16. The developed sensor demonstrates a reduced sensitivity towards CO₂ and SO₂ compared to NO₂ at different temperatures. At a temperature of 100 °C, the sensor exhibits a sensitivity of approximately five times greater, indicating that the proposed sensor has higher selectivity against NO₂.

5. Conclusions

A good specification and low-cost NO₂ gas sensor have been prepared based on porous silicon decorated with ZnO nanoparticles by PLD technology. FE-SEM images and EDS analysis indicate a homogeneous distribution of ZnO NPs on porous silicon without closing the surface pores, significantly affecting the gas sensitivity. The gas sensor specification is improved for the sample deposited on PSi compared to the sample deposited on the Si wafer. The optimum sensitivity was 75.3% at an operating temperature of 100 °C, and the response time was about 25 s for ZnO/PSi and 32 s for ZnO/Si. The developed sensor's sensitivity corresponds to the proposed relationship, which can be used to design quantitative gas sensors. At 100 °C, the ZnO/PSi sensor exhibited selectivity towards NO₂ approximately five times.

Funding The authors confirm that the present manuscript has not received any financial support from any organization or individual apart from the authors.

Declarations

Conflict of interest The authors declare that they have no known competing financial interests or personal relationships that could have influenced the work reported in this paper.

Novelty statement In this study, the detection of low nitrogen dioxide concentrations was applied using the pulsed laser deposition method to deposit zinc oxide nanoparticles on a silicon substrate. A fast, low-cost, effective, and safe method was used to etch the silicon substrate to enhance the zinc oxide film's sensitivity characteristics. In addition to studying the etching influences on the sensitivity characteristics of ZnO, the interaction mechanism between the gas and the surface of the sensor was addressed. Finally, the effect of increasing the nitrogen dioxide concentration on the sensing characteristics of the deposited films was analyzed. A relation between sensitivity and gas concentration was proposed based on the obtained results of the sensor, and it demonstrated a good agreement with the study's findings.

References

- [1] S M Majhi, A Mirzaei, H W Kim, S S Kim and T W Kim *Nano Energy* **79** 105369 (2021)

- [2] I M Ibrahim, J M Rzaiz and A Ramizy *Dig. J. Nanomater. Biostructures* **12** 1187 (2017)
- [3] J M Marei, A A Khalefa and Q A Abduljabbar *J. Nano Res.* **70** 41 (2021)
- [4] A Patil and C Dighavkar *J. Optoelectron. Adv. Mater.* **13** 1331 (2011)
- [5] S Khoshnevis, R S Dariani, M E Azim-Araghi, Z Bayindir and K Robbie *Thin Solid Films* **515** 2650 (2006)
- [6] A M Alwan and H R Abed *State. Electron.* **181–182** 108019 (2021)
- [7] D H Jwied, U M Nayef, and F A H Mutlak, *Optik (Stuttg).* **242** 167207 (2021)
- [8] M Bahar and H Eskandari *J. Theor. Comput. Sci.* **04** 2 (2017)
- [9] A Kumar, A Kumar, R Chandra *Sensors Actuators B Chem.* **264** 10 (2018)
- [10] G Modi *Adv. Nat. Sci. Nanosci. Nanotechnol.* **6** 033002 (2015)
- [11] A B Khatibani *Indian J. Phys.* **95** 243 (2021)
- [12] G Hui, M Zhu, X Yang, J Liu and G Pan *Mater* **278** 128453 (2020)
- [13] C Zhang, Y Luo, X Chen, W Ou-Yang, Y Chen and Z Sun *Surf. Sci.* **388** 82 (2016)
- [14] B S Mwankemwa, S Akinkuade, K Maabong and J M Nel *B Condens. Matter* **535** 175 (2018)
- [15] P Caban, R Pietruszka, K Kopalko, B S Witkowski, K Gwozdz, E Placzek-Popko, and M Godlewski *Optik (Stuttg).* **157** 743 (2018)
- [16] H Makino and H Shimizu *Appl. Surf. Sci.* **439** 839 (2018)
- [17] S Denchitharoen and N Siriphongsapak *Today Proc.* **4** 6146 (2017)
- [18] D Nesheva, V Dzhurkov, I Stambolova, V Blaskov and I Bineva *Chem. Phys.* **209** 165 (2018)
- [19] M G Tsoutsouva, C N Panagopoulos, D Papadimitriou and I Fasaki *Sci. Eng. B* **176** 480 (2011)
- [20] K K Jasmi *Today Proc.* **65** 3610 (2022)
- [21] R C Ramola, S Negi and R C Singh *Rep.* **12** 22351 (2022)
- [22] B Ghanbari Shohany, L Motevalizadeh, and M Ebrahimizadeh Abrishami *J. Theor. Appl. Phys.* **12** 219 (2018)
- [23] D Fasquelle *V Bouquet, and M Guilloux-Viry Chemosensors* **10** 285 (2022)
- [24] M K Ibraimov, Y Sagidolda, S L Rumyantsev and Z Z Zhanabaev *Lett.* **14** 588 (2016)
- [25] A Kumar, A Sanger, A Kumar, and R Chandra *RSC Adv.* **7** 39666 (2017)
- [26] A M Alwan and D A Hashim *J. Mater. Sci. Mater. Electron.* **30** 7301 (2019)
- [27] F Ramírez-González, G García-Salgado, E Rosendo, T Díaz, F Nieto-Caballero, A Coyopol, R Romano, A Luna, K Monfil, and E Gastellou *Sensors* **20** 4942 (2020)
- [28] J M Rzaiz and N F Habubi *Appl. Phys. A Mater. Sci. Process.* **126** 560 (2020)
- [29] R Kumar, O Al-Dossary, G Kumar, and A Umar *Nano-Micro Lett.* **7** 97 (2015)
- [30] J M Rzaiz, A S Ibraheam, and A M Abass *Baghdad Sci. J.* **18** 401 (2021)
- [31] A S Ibraheam and J M Rzaiz *J. Electron. Mater.* **52** 414 (2023)
- [32] J Ding, L Ge, X Zhu, J Jiao and L Zhang *J. Phys. Chem. A* **95** 2663 (2021)
- [33] M Pavlenko, V Myndrul, G Gottardi, E Coy, M Jancelewicz, and I Iatsunskyi *Materials (Basel).* **13** 1987 (2020)
- [34] R Venkatesan, J Mayandi and J M Pearce *J. Mater. Sci. Mater. Electron.* **30** 8676 (2019)
- [35] F Morales-Morales, A Benítez-Lara, N Hernández-Sebastián, F Ambriz-Vargas, M R Jiménez-Vivanco and R López *Sci. Semicond. Process.* **148** 106810 (2022)
- [36] X Wei, R Zhao, M Shao and X Xu *Lett.* **8** 112 (2013)
- [37] L Martínez, O Ocampo and Y Kumar *Lett.* **9** 437 (2014)
- [38] J Hernandez-Montelongo, A Munoz-Noval, J P Garca-a-Rua-z, V Torres-Costa, R J Marta-n-Palma, and M Manso-Silvan *Front. Bioeng. Biotechnol.* **3** 1 (2015)
- [39] Q A Abduljabbar, H A Radwan and J M Marei *Res. Express* **4** 015028 (2022)
- [40] F-Z Tebizi-Tighilt, F Zane, N Belhaneche-Bensemra, S Belhousse and S Sam *Surf. Sci.* **269** 180 (2013)
- [41] G K Mani and J B B Rayappan *Sensors Actuators B Chem.* **198** 125 (2014)
- [42] J M Rzaiz and N F Habubi *J. Mater. Sci. Mater. Electron.* **33** 11851 (2022)
- [43] Y F Sun, S B Liu, F L Meng, J Y Liu, Z Jin, L T Kong, and J H Liu *Sensors* **12** 2610 (2012)
- [44] H Xuemei and S Yukun *J. Nanomater.* **2016** 1 (2016)
- [45] K Schneider and W Maziarz *V2O5 Thin Films as Nitrogen Dioxide Sensors* (Basel Switzerland : MDPI) p. 759 (2018)
- [46] A A Khalefa, J M Marei and H A Radwan *J. Nanomater. Biostructures* **16** 197 (2021)

Publisher's Note Springer Nature remains neutral with regard to jurisdictional claims in published maps and institutional affiliations.

Springer Nature or its licensor (e.g. a society or other partner) holds exclusive rights to this article under a publishing agreement with the author(s) or other rightsholder(s); author self-archiving of the accepted manuscript version of this article is solely governed by the terms of such publishing agreement and applicable law.